Table 9.4: PHENIX Electromagnetic Calorimetry: Performance Summary

Characteristic	PbSc	PbGl
Energy Range (GeV)		
Au + Au collisions	0.1–50	0.1–50
p + p collisions	0.1–50	0.1–50
Least count (GeV)	0.002	0.002
Dynamic Range	15-bit (12+3)	15-bit (12+3)
Energy Resolution %	$8/\sqrt{E} \oplus 1.5$	$5.8/\sqrt{E} \oplus 1.$
Timing Resolution (ns)	$0.07 + 2.7/\sqrt{N_{pe} \cdot E_{Dep}}$	$0.075 + 3.75/\sqrt{N_{pe} \cdot E_{Dep}}$
Spatial Res., σ_x (mm)	$< 10./\sqrt{E(GeV)}$	$(5./\sqrt{E(GeV)} + 1.)$

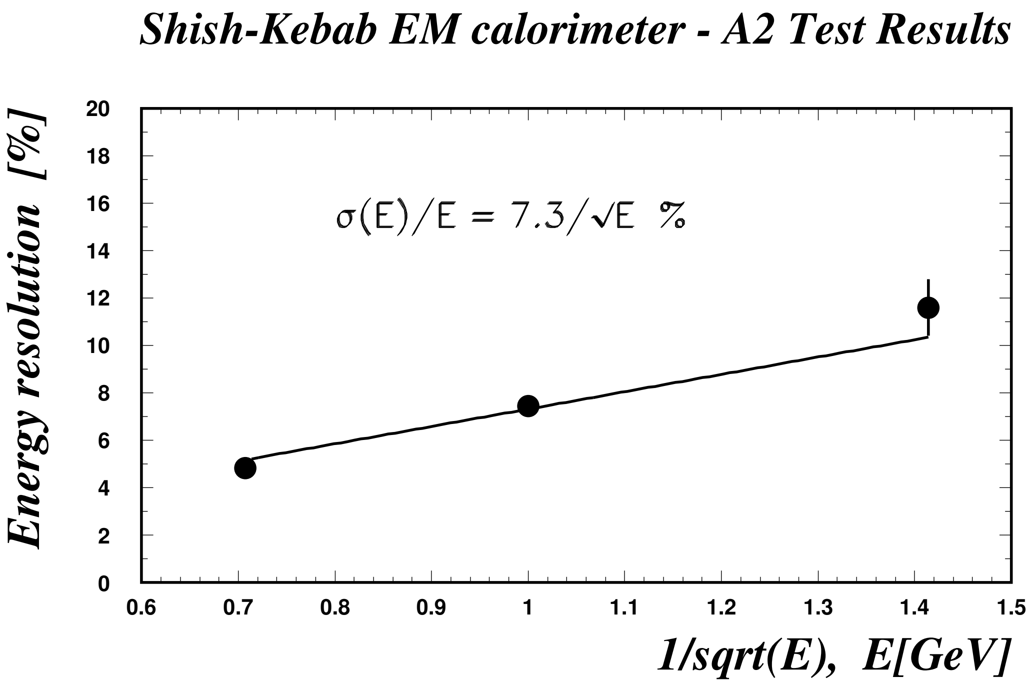

Figure 9.8: Energy resolution of PbSc (shish-kebab) calorimeter measured in the 1992 test for electrons of different momenta.

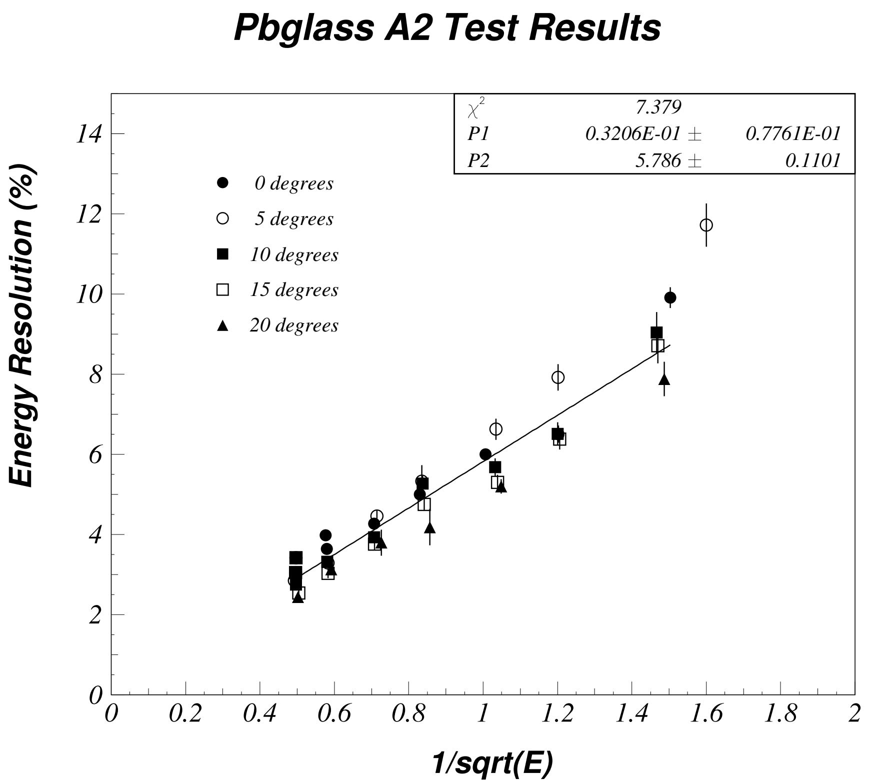

Figure 9.9: Energy resolution of PbGl calorimeter for electrons with incident momenta 0.5–4.0 GeV/c at various angles of incidence.

particle deposits energy in the calorimeter. The time resolution is approximately equal to 100 ps for electrons and penetrating particles in both calorimeters, close to that value for showering hadrons in the PbGl calorimeter, and around 230 ps for showering hadrons in the PbSc calorimeter.

The second term in Eq. 9.1 involves the effective signal risetime and the number of photo-electrons, N_{pe}, per GeV of deposited energy, E_{dep}. For the PbGl, the light collection presumably occurs over a time interval of the order of one ns or less. Thus for PbGl, δt_1 simply reflects the photomultiplier risetime and is found to be about one-third to one-fourth of the photomultiplier risetime. The measured time resolution for PbGl is shown in Fig. 9.10. A value of $\delta t_1 = 3.75$ ns is obtained for PbGl when using the FEU-84 photomultiplier, which has a risetime of 10–15 ns. A faster (shorter risetime) photomultiplier is expected to directly improve δt_1.

Because the signal risetime in a PbSc calorimeter is a convolution of the scintillator decay time together with the photomultiplier risetime the effective signal risetime is not entirely due to the photomultiplier. Depending on the choice of scintillator, the effective signal risetime can be slower than the phototube risetime by as much as a factor of two. On the other hand, our PbSc modules have a larger value of N_{pe} than the PbGl value. A yield of $N_{pe} = 1300$

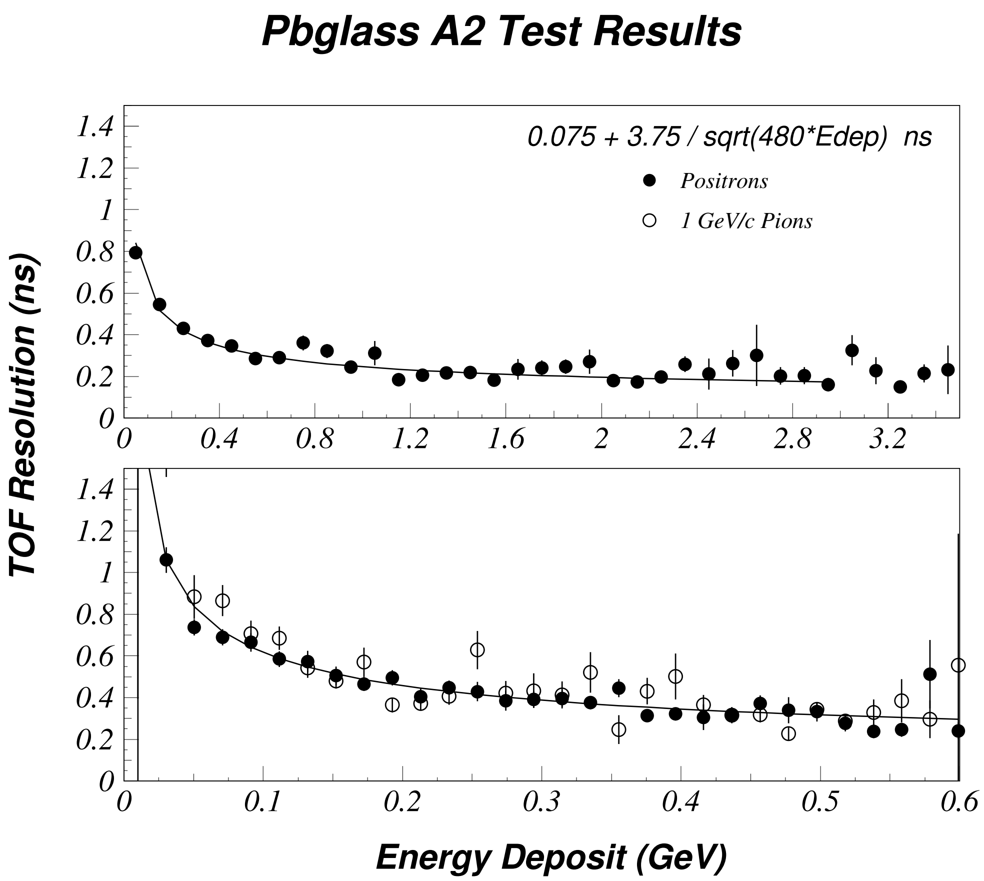

Figure 9.10: Single PbGl module timing resolution as a function of the energy deposited in the module for electrons with incident momenta 0.5–4.0 GeV/c and for pions of 1.0 GeV/c.

per GeV of energy deposit was measured for the basic PbSc configuration (Russian injection molded fast scintillator + G2 wavelength shifter fiber + FEU-84 photomultiplier), whereas an average value of $N_{pe} = 620$ was obtained for the PbGl with the FEU-84 photomultiplier. Due to the intrinsically short signal pulse in the PbGl nearly 50% of the photoelectrons are associated with the leading edge of the signal. On the other hand, the corresponding fraction of the photoelectrons in the PbSc pulse leading edge is about 30% for a very fast scintillator, but decreases to about 20% for a relatively slow scintillator. A combination of the effects involved results in a typical value of $\delta t_1 \simeq 2.7$ ns measured with a fast tube (see Fig. 9.11). This is rather similar to that measured for the PbGl calorimeter equipped with the slow FEU84 photomultipliers.

There is one apparent result from timing measurements with the calorimeter, which is common for PbSc and PbGl, and which complicates the interpretation of the time-of-flight capability. The leading edge of the photomultiplier pulse is delayed with respect to the time at which the particle arrives by the time needed for the shower to develop and for the light to propagate to the PMT. In general this delay depends on the shower development (and thus

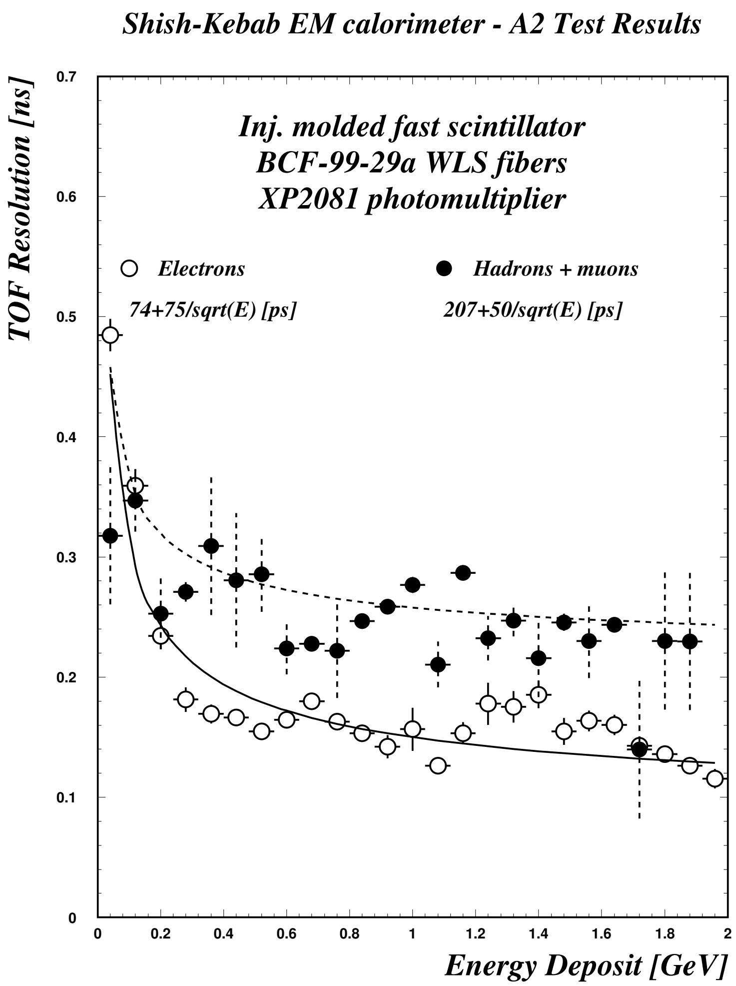

Figure 9.11: Single shish-kebab module timing resolution (rms) vs. equivalent energy deposited in the module for electrons and pions of incident momenta 0.5 to 2.0 GeV/c.

on the nature of the showering particle) and on its kinetic energy (which determines how deep the shower propagates into the calorimeter). Above 500 MeV/c electrons appear to be late compared to showering hadrons, which are in turn earlier than non-showering hadrons and muons. This difference tends to disappear as the momentum increases. Experimental data are not yet available for momenta below 500 MeV/c so the time-of-flight performance of the calorimeter for low momentum particles must be predicted by GEANT simulation which was tuned to reproduce the test beam results at higher momenta. The time delay in the PbSc calorimeter as computed from GEANT simulation for electrons, showering pions, and muons and non-showering pions is plotted versus particle incident momentum in Fig. 9.12.

The insert in Fig. 9.12 shows the momentum dependence of the intrinsic time-of-flight resolution of the calorimeter computed as an rms of the time delay in a given momentum bin. A striking feature of these results is the consistency between the experimentally deter-

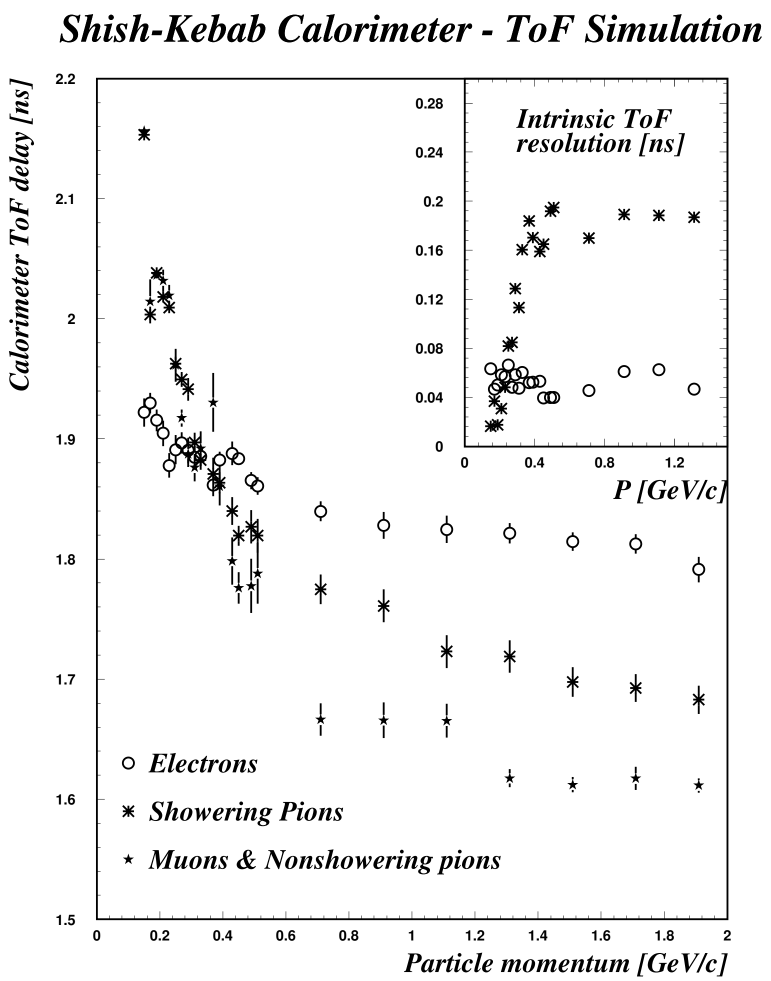

Figure 9.12: GEANT simulation of the timing response of the PbSc showing the timing delay as a function of incident momentum for electrons, showering pions, and muons and non-showering pions. Insert: intrinsic time-of-flight resolution for electrons and pions as predicted by GEANT.

mined constant term and the GEANT predictions for the intrinsic calorimeter time-of-flight resolution. There is a general tendency for a larger delay in signal arrival time at low momenta. All three curves cross in the region where pions stop in the calorimeter with the electron signal arrival time then becoming the earliest. Further R&D is planned to perform a more complete study of the calorimeter time-of-flight response at low incident momenta.

9.4.3 Electron Identification

Discrimination between e and π in the electromagnetic calorimeter is primarily achieved by the comparison of deposited energy to the measured track momentum. Thus its effectiveness depends on the calorimeter energy resolution as well as on the calorimeter response to